Contactless electro-reflectance study of interdiffusion in heat-treated $GaAs_{1-x}Sb_x/GaAs$ single quantum wells

1998 J. Phys.: Condens. Matter 10 9865

(http://iopscience.iop.org/0953-8984/10/43/031)

J. Phys.: Condens. Matter **10** (1998) 9865–9874. Printed in the UK PII: S0953-8984(98)93219-2

Contactless electro-reflectance study of interdiffusion in heat-treated $GaAs_{1-x}Sb_x/GaAs$ single quantum wells

Sandip Ghosh†+, B M Arora†, K P Homewood‡, W P Gillin§, O M Khreis‖ and K E Singer¶

† Solid State Electronics Group, Tata Institute of Fundamental Research, Homi Bhabha Road, Colaba, Mumbai 400 005, India

‡ School of Electronic Engineering, Information Technology and Mathematics, University of Surrey, Guildford, Surrey GU2 5XH, UK

§ Department of Physics, Queen Mary and Westfield College, Mile End Road, London E1 4NS, UK

‖ Hijjawi faculty for Engineering and Technologies, Yarmouk University, Irbid, Jordan

¶ Department of Electrical Engineering and Electronics, University of Manchester Institute of Science and Technology, Manchester M60 1QD, UK

Received 7 April 1998

Abstract. We have studied the interdiffusion process on the group V sublattice in thermally annealed, undoped $GaAs_{1-x}Sb_x/GaAs$ strained single quantum wells by comparing the results of contactless electro-reflectance spectroscopy with theoretically estimated optical transition energies. We show that the interdiffusion process in this system is Fickian. We estimate the activation energy for the interdiffusion process to be 1.5 ± 0.2 eV, which is low compared to those reported for other III–V-alloy-based heterostructures.

1. Introduction

Studies on interdiffusion of atoms across the interfaces of $GaAs_{1-x}Sb_x/GaAs$ quantum wells (QW) are important for the following two main reasons. This system is a promising material for infrared optoelectronic device applications so the knowledge of the interdiffusion process is of crucial importance from the point of view of device processing. Secondly although the interdiffusion process on the group III sublattice in systems such as $Al_{1-x}Ga_xSb/GaAs$ QW has been extensively studied [1], few such studies exist on the interdiffusion process on the group V sublattice. Recent work by Egger *et al* [2] suggests that the interdiffusion process in the $GaAs_{1-x}Sb_x/GaAs$ system obeys Fick's second law of diffusion, contradicting an earlier report of Gillin *et al* [3] which claimed that this process was highly non-linear. These contradictory results leave scope for further study.

The change in the concentration profile of the atoms due to interdiffusion has been studied by direct measurements, such as tunnelling electron microscopy (TEM) and secondary-ion mass spectrometry (SIMS), and by indirect optical spectroscopic means, such as photoluminescence (PL), and these have been reviewed by Deppe and Holonyak [1]. In the indirect approach [4] the optical transition energies are measured after the interdiffusion has taken place. These are then compared with theoretical transition energies obtained by considering model interdiffusion processes to determine the parameters associated with

+ Present address: Department of Physics, University of Surrey, Guildford, Surrey GU2 5XH, UK.

0953-8984/98/439865+10$19.50

the interdiffusion process in the sample. In our study we have adopted this approach but instead of PL we have used contactless electro-reflectance (CER) spectroscopy to determine the optical transition energies in $GaAs_{1-x}Sb_x$/GaAs QW samples which were subjected to rapid thermal annealing treatments in order to induce interdiffusion. The use of CER is particularly advantageous in the study of QW structures [5] as it can reveal transitions between the higher-lying states of the QW which are normally inaccessible to PL and therefore can provide a further check on the well shape to determine whether the process is Fickian. Also CER is largely insensitive to defects and measures the exact band-edge transition energies which in the case of PL may at times become difficult due to the presence of dominant defect-related features in the spectrum.

2. Experimental details

The samples used in this study were grown by molecular beam epitaxy (MBE) on semi-insulating (001) GaAs substrates. The sample structure consisted of a buffer GaAs barrier layer on the substrate that was not intentionally doped, and a $GaAs_{1-x}Sb_x$well layer with a nominal thickness of 100 Å and Sb concentration (x^0) of 11% followed by another 300 Å GaAs barrier layer on top. The samples were then capped with a 500 Å layer of silicon nitride grown at 300 °C in a plasma-enhanced chemical vapour deposition system. The wafers were cut into 5×5 mm^2 squares for the annealing experiments. Annealing was performed in a helium ambient using a resistively heated graphite strip heater. The annealing furnace was calibrated against the melting points of gold and silver and found to be accurate to ±1 °C. This system has a rise time of ∼2 s from 700 °C to 1000 °C and a fall time of ∼4 s over the same temperature range. Of the four samples on which the measurements were performed, the first was the as-grown unannealed sample (S1), the second was annealed at 800 °C for 420 s (S2), the third was annealed at 900 °C for 280 s (S3) and the fourth at 1000 °C for 220 s (S4).

In the CER [6] measurements the samples were placed between two electrodes in a capacitor like arrangement with the top electrode kept ∼0.3 mm from the sample surface. A maximum of 3.5 kV (pp) sinusoidal voltage (at 330 Hz) was applied to the top transparent electrode (ZnO film on glass) for the purpose of modulation [7]. The probe beam was obtained by dispersing light from a 150 W quartz tungsten halogen lamp using a 1/8 m monochromator with ∼4 nm band-pass and detected using a silicon photodetector. Phase-sensitive detection of the modulated reflectivity signal was carried out using a lock-in amplifier. The samples were cooled using a closed-cycle He refrigerator.

3. Theoretical estimation of the transition energies

The interdiffusion process involves the out-diffusion of Sb from the well region into the barrier region and the simultaneous in-diffusion of As into the well region from the barrier region of the QW. The process can be quantified by the change in the Sb concentration profile [4], which is initially a constant ($=x^0$) in the well region and zero in the adjacent barrier GaAs layers. For such a situation, assuming that the diffusion process obeys Fick's second law, the modified Sb concentration profile is given by an error-function-defined solution as

$$x(z) = x^0 \frac{1}{2}\left[\operatorname{erf}\left(\frac{(L_w/2) - z}{L_d}\right) + \operatorname{erf}\left(\frac{(L_w/2) + z}{L_d}\right)\right] \qquad L_d = 2\sqrt{Dt} \tag{1}$$

where z is the direction perpendicular to the plane of the well, $z = 0$ being the centre of the QW, $L_w \equiv$ initial QW width, $L_d \equiv$ diffusion length, $D \equiv$ interdiffusion coefficient and t is the duration of the heat treatment. The change in the Sb concentration profile modifies the QW potential profile. To determine this changed band-gap profile we have combined the Varshini expression for temperature dependence [8] and the quadratic expression for Sb concentration dependence [8] of the unstrained band gap of the $GaAs_{1-x}Sb_x$ alloys, which results in

$$Eg_0(x, T) = 0.810 - \frac{3.78 \times 10^{-4}T^2}{(T + 94)} - 0.502(1 - x) + 1.2(1 - x)^2 + [(1 - x)(0.013\,19 - 1.242 \times 10^{-7}T^2)]. \quad (2)$$

Table 1. Values of physical parameters of GaAs and GaSb used in calculations to obtain the theoretical optical transition energies in the quantum wells.

Parameter	GaAs	GaSb
Lattice constant a^L (Å)	5.6533	6.0959
Spin–orbit splitting (eV)	0.341	0.747
Electron effective mass (m^*/m_0)	0.067	0.041
Luttinger parameter γ_1	6.85	13.3
Luttinger parameter γ_2	2.1	4.4
Hydrostatic deformation potential $a_{(VB+CB)}$ (eV)	−9.22	−8.3
Shear deformation potential $a_{(VB+CB)}$ (eV)	−2.0	−1.9
Elastic constant C_{11} (10^{11} dyn cm^{-2})	11.9	8.83
Elastic constant C_{12} (10^{11} dyn cm^{-2})	5.38	4.02

The last expression in the square brackets is a small correction which makes the above equation follow the temperature-dependent band-gap variation of GaAs for $x = 0$ and that of GaSb for $x = 1$. Due to lattice mismatch between GaAs and GaSb, the $GaAs_{1-x}Sb_x$ well layer is expected to be under compressive strain. To account for the effect of this strain on the band gap of the alloy layer we considered the following relation which determines the heavy-hole (hh) and the light-hole (lh) band gaps at the Γ point in the reciprocal space of direct-gap semiconductors with zinc-blende structure [9]:

$$Eg_{hh} = Eg_0 + \delta h + \delta s \qquad Eg_{lh} = Eg_0 + \delta h + \frac{1}{2}(\Delta - \delta s) + \frac{1}{2}\sqrt{\Delta^2 + 2\Delta\,\delta s + 9(\delta s)^2} \quad (3)$$

with

$$\delta h = 2fa\frac{C_{11} - C_{12}}{C_{11}} \qquad \delta s = -fb\frac{C_{11} + 2C_{12}}{C_{11}} \qquad f = \frac{a^L_{GaAs} - a^L_{alloy}}{a^L_{alloy}}$$

where $\Delta \equiv$ the spin–orbit split-off energy of the alloy, $C_{ij} \equiv$ elastic constants of the alloy, $a^L_{GaAs}, a^L_{alloy} \equiv$ lattice constants, f is the strain parameter determined by assuming that the $GaAs_{1-x}Sb_x$ alloy layer is coherently strained with respect to GaAs; a and b are the deformation potentials of the alloy. The values of these parameters, including the carrier effective masses which are to be used subsequently, for a particular x were obtained by appropriate interpolation between the listed values of these parameters [10] for GaAs and GaSb (see table 1). The band alignment for this system has been shown [11] to be of type I, and since it is known that the conduction–valence band offset ratio does not significantly affect the transition energies, it was taken to be 50:50 in our work. Knowing

the potential profile, the optical transition energies can be calculated by determining the carrier confinement energies in the well. In the envelope wavefunction approximation this problem reduces to solving the one-dimensional Schrödinger equation which in the present case was accomplished numerically using the tunnelling resonance technique described in the appendix. The actual transition energies are expected to be lower by an amount equal to the exciton binding energy whose upper limit was estimated [12] to be 6.2 meV for the hh exciton and 4.6 meV for the lh exciton for the square-well potential.

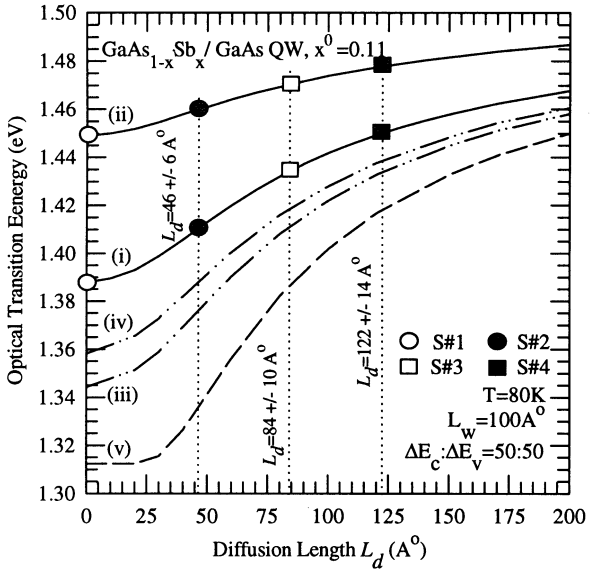

Figure 1. Calculated optical transition energies as a function of diffusion length. Plots: (i) the e1–hh1 transition considering strain, quantum confinement and exciton binding energy, (ii) the e1–lh1 transition with the same considerations, (iii) e1–hh1 considering confinement but no strain, (iv) e1–lh1 considering confinement but no strain, (v) the lowest-energy transition considering no quantum confinement and no strain. The symbols are placed where the two measured transition energies in a sample meet plot (i) and (ii). L_d for the sample is determined from the intersection of the vertical dotted line through a symbol with the x-axis.

Plots (i) and (ii) in figure 1 show the variation with L_d in the calculated energies of the transitions to the first confined electron level in the conduction band from the first confined hh level (e1–hh1) and the first confined light-hole level (e1–lh1) in the valence band respectively. These transitions are expected to be the most prominent. Also plotted are these two transition energies without taking into account the strain (plots (iii) and (iv)) and a case where neither strain nor confinement was accounted for (plot (v)). It is evident that the transition energies are quite different when shifts due to strain and confinement are neglected, as was done by Egger *et al* [2], from the case in which they are taken into account.

4. Results and discussion

Figure 2 shows the CER spectrum of the unannealed sample at three different temperatures. At 295 K the structure in the spectrum beyond 1.39 eV is due to the GaAs barriers while the other two features at lower energies are the signatures of the QW. The GaAs feature,

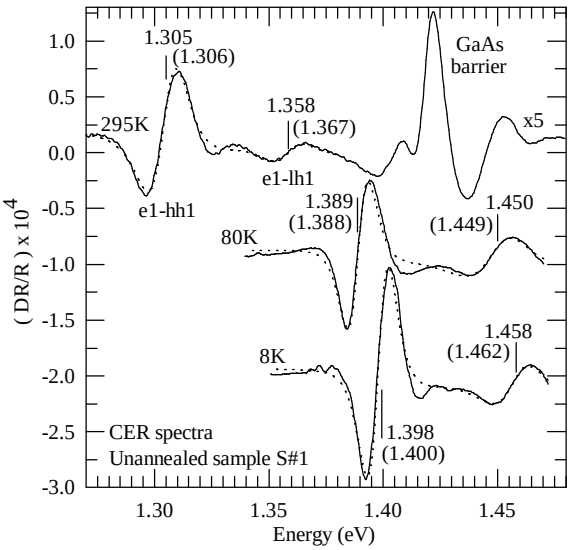

Figure 2. The CER spectra of the unannealed square well at three different temperatures. The vertical lines and the unbracketed numbers indicate the positions of the experimentally obtained transition energy while the calculated transition energies are given in brackets. The dotted lines show the fitted lineshapes. The plots are shifted vertically for clarity.

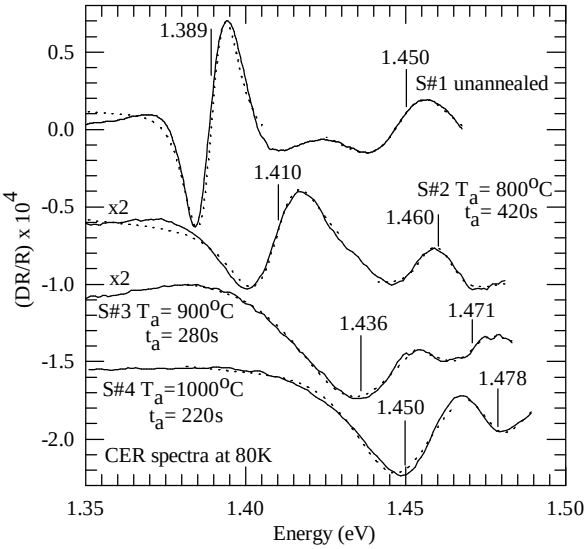

Figure 3. CER spectra of the four samples at 80 K. The numbers and the vertical lines indicate the experimentally obtained transition energies having a maximum uncertainty of ±4 meV. The dotted lines show the separately fitted lineshapes. The plots are vertically shifted for clarity.

being unimportant in the present context, has not been shown in the other spectra; instead the QW signatures have been emphasized. At 295 K the QW-related features at 1.306 eV and 1.358 eV are identified as e1–hh1 and e1–lh1 transitions respectively which move up in energy as the temperature is lowered due to increase in the band gap of the well and the

barrier layers. The transition energies (unbracketed numbers) were estimated by fitting the following lineshape function to these spectral features:

$$\frac{\Delta R}{R}(E) = \sum_{j=1}^{n} \mathrm{Re}\left[a_j \exp(\mathrm{i}\theta_j)/(E - E_{0j} + \mathrm{i}\Gamma_j)^m\right] \qquad \mathrm{i} = \sqrt{-1} \tag{4}$$

where E_{0j}, Γ_j, θ_j and a_j are the transition energy, broadening parameter, phase factor and amplitude respectively, associated with the jth transition. In the above equation the value used for the exponent m was 3 which mimics the case of a first-derivative Gaussian-broadened lineshape function [5] applicable in the case of the inhomogeneously broadened dielectric function of quantum confined systems. The fitted spectra are shown by dotted lines. It is evident that the agreement between the measured transition energies (unbracketed numbers) and the calculated ones (bracketed numbers) is reasonably good, which validates the use of the above procedure and the parameters for the theoretical estimation of the transition energies. It is seen from figure 1 that the separation between the e1–hh1 and the e1–lh1 transition energies is very sensitive to the presence of strain. Our experimentally measured values do not match the theoretical values unless strain is taken into account, indicating that the QW layer is strained. This is in accordance with the fact that the QW layer thickness is less than the critical thickness for strain relaxation for $GaAs_{0.89}Sb_{0.11}$ layers on GaAs. We note that it would not be possible to detect the e1–lh1 transition in PL with such a large difference between the e1–hh1 and e1–lh1 transition energies.

Figure 3 shows the 80 K CER spectra of the samples which were subjected to heat treatment. The lineshapes are significantly modified, getting appreciably broadened due to inhomogeneous change in the Sb profile in the plane of the sample. However, as expected, the QW-related features move up in energy with heat treatment. This is because the out-diffusion of Sb makes the QW shallower and therefore the transition energy tends to move closer to the barrier band gap. The lineshape function in equation (4) was fitted to these broadened hh- and lh-related spectral features separately in order to estimate the transition energies. The experimental transition energies are indicated by the numbers in figure 3. Using the values shown in figure 3, symbols have been placed in figure 1 where the two measured transition energies e1–hh1 and e1–lh1 of a sample meet plots (i) and (ii) respectively. Thereafter L_d is determined by the intersection of a vertical line through the two symbols with the x-axis in figure 1. We find that for any one of the three annealed samples, both the e1–hh1 and e1–lh1 transitions give one unique value of L_d. This means that the changes in the potential profile due to the annealing treatment are indeed following the potential profile resulting from equations (1)–(3). Had this not been the case then the lh and hh transition energies would not simultaneously follow the plots (i) and (ii) of figure 1 and we would get two significantly different values of L_d for a given sample. Thus these results show that the interdiffusion process is indeed Fickian. Our results also show that no catastrophic strain relaxation has occurred during the annealing process as this would have shown up prominently as an abrupt change in the e1–hh1 and e1–lh1 transition energy separation.

From the L_d-values, the interdiffusion coefficients were estimated using $D = L_d^2/4t_a$ where t_a is the duration of the annealing. The error in D was estimated from the error in estimating L_d using figure 1 considering a ± 4 meV error in determining the experimental transition energies. Figure 4 shows a plot of D versus the inverse of the annealing temperature. Our data (circles) were fitted to an Arrhenius relation of the type $D = D_0 \exp(-Q/k_B T)$ which gave $Q = 1.5 \pm 0.2$ eV and $D_0 = (2.2^{+6.6}_{-1.7}) \times 10^{-9}$ cm^2 s^{-1}. Also shown in figure 4 (triangles) are recent estimates of the interdiffusion coefficient for this system based on PL measurements by Khreis *et al* [13] who obtain a value of 2.0 ± 0.2 eV

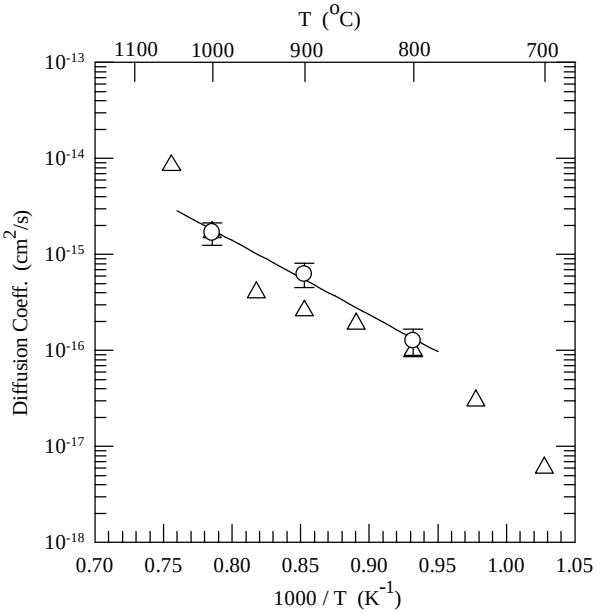

Figure 4. An Arrhenius plot of the dependence of the diffusion coefficient on the annealing temperature. The continuous line is a fit to our data (circles). The data of Khreis *et al* [13] (triangles) on this system, based on photoluminescence measurements, are also shown for comparison.

for Q. The agreement between these two independent estimates of the interdiffusion coefficient for the $GaAs_{1-x}Sb_x/GaAs$ system is evidently quite good. These authors have also suggested that the non-linear diffusion process reported earlier by Gillin *et al* [3] may have been due to an excessively high initial non-equilibrium concentration of point defects in their samples.

Atomic interdiffusion across heterointerfaces in most III–V semiconductors is believed to be mediated by the vacancy point defects. This conclusion is primarily based on a comparison of the activation energy for the interdiffusion process with self-diffusion of the group III and V elements in these materials. For example the activation energy for interdiffusion on the group V sublattice in the quaternary $In_\delta Ga_{1-\delta}As_{1-x}P_x/In_\delta Ga_{1-\delta}As$ system is reported to be ∼3.7 eV [14], while for the $GaAs_{1-x}P_x/GaAs$ system its value is found to be ∼4.1 eV [2]. These values of the activation energy are close to that for As self-diffusion in GaAs which is known to be governed by the group V vacancy mechanism [15], thereby suggesting that a similar mechanism is operative in the above-mentioned systems. Our estimate of $Q \sim 1.5$ eV for the $GaAs_{1-x}Sb_x/GaAs$ system is considerably lower in comparison. Such low values of activation energy have been reported earlier by Tsang *et al* [16] for interdiffusion on the group III sublattice in the $In_xGa_{1-x}As/GaAs$ system ($Q \sim 1.63$ eV); they propose a diffusion mechanism based on an enhanced non-equilibrium vacancy concentration for lowering of the effective Q-value. Given the evidence that it is possible to have similar mechanisms for interdiffusion on group III and group V sublattices with nearly identical activation energies [17], one may be tempted to suggest by comparison with the work of Tsang *et al* that the low value of Q in the present case also indicates an enhanced non-equilibrium group V vacancy mechanism at play here. However, one must keep in mind that in the work of Tsang *et al*, a low-

temperature-grown GaAs cap layer (LT-GaAs) was deliberately put on the sample. The LT-GaAs is rich in defects and acted as an internal source of vacancies. On the other hand, in our samples, the silicon nitride cap is expected to prevent the loss of As from the surface during the heat treatment. Therefore it is not clear what the source of the non-equilibrium concentration of vacancies could be in the present case. Thus while the nature of the diffusion process is shown to be Fickian in the $GaAs_{1-x}Sb_x$/GaAs system, the exact microscopic mechanism remains uncertain, which calls for further experiments to provide a better understanding.

5. Conclusion

In summary, by taking advantage of CER spectroscopy which enabled us to track the variation in the energy of more than one transition associated with QWs subjected to thermal annealing, we have shown that the interdiffusion process in the $GaAs_{1-x}Sb_x$/GaAs system is indeed Fickian. This clears up any doubts about a non-Fickian process giving rise to erroneous results. The interdiffusion coefficient in the range 800 °C to 1000 °C has been measured. The value of the activation energy for the interdiffusion process is found to be low, which cannot be explained on the basis of mechanisms proposed for other III–V-alloy-based heterostructures.

Acknowledgments

The authors SG and BMA would like to thank Professor K L Narsimhan and Professor S Chandrasekaran for many useful discussions.

Appendix

The tunnelling resonance technique, also referred to as the transfer-matrix technique, is based on the principle that when a particle is incident on a potential structure consisting of a double barrier with a well in between, its transmission coefficient peaks for certain incident energies which, in the limit of large barrier widths, correspond to the eigenstate energies in the well. This technique can be used to determine the eigenvalues of an arbitrarily shaped finite one-dimensional potential. Here the actual QW potential profile is approximated by a series of finite-height rectangular wells with two barriers, of finite height and width, on either end as shown in figure A1(a). The transmission coefficient of this structure is then calculated by numerically solving the time-independent Schrödinger equation given by

$$\frac{\mathrm{d}^2\phi}{\mathrm{d}x^2} + \frac{2m^*}{\hbar^2}[E - V(x)]\phi = 0$$

where ϕ is the envelope wavefunction, m^* is the particle's effective mass (for the valence band, $m^* = m_0(\gamma_1 \mp 2\gamma_2)^{-1}$, for heavy holes (hh) and light holes (lh) respectively; $m_0 \equiv$ free-electron mass, $\gamma_{1,2} \equiv$ Luttinger parameters), $\hbar$ is Planck's constant, E is the eigenvalue and $V(x)$ is the potential profile. Its solution in the jth well of thickness d_j, potential height V_j and effective mass m_j^* can be written as [18]

$$\phi_j = \phi_j^+ \mathrm{e}^{-\mathrm{i}\Delta_j}\mathrm{e}^{\mathrm{i}k_j x} + \phi_j^- \mathrm{e}^{\mathrm{i}\Delta_j}\mathrm{e}^{-\mathrm{i}k_j x} \tag{A1}$$

where

$$\Delta_1 = \Delta_2 = 0$$

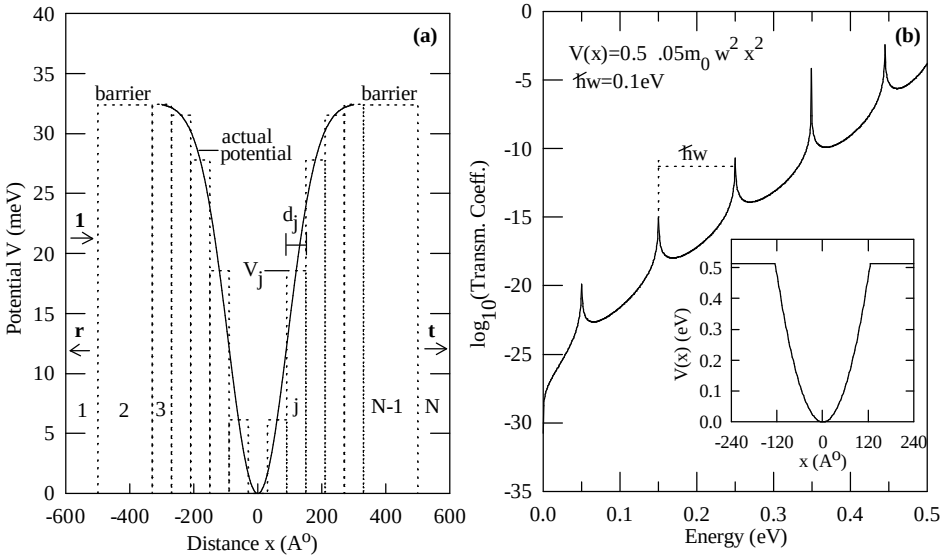

Figure A1. (a) A typical error-function-defined potential (equations (1)–(3); $L_d = 122$ Å) shown by the continuous line, being approximated by a series of finite square wells (dotted line). (b) The solution for a test case with a finite parabolic potential (inset). The energy positions of the peaks in the transmission coefficient show the characteristic $(n + \frac{1}{2})\hbar\omega$ behaviour.

$$\Delta_j = k_j \sum_{l=2}^{j-1} d_l \qquad \text{where } k_j = \sqrt{\frac{2m_j^*}{\hbar^2}[E - V_j]}.$$

$\phi_j^{\pm}$ are the amplitudes of the positive- and the negative-going waves ($\mathrm{i} = \sqrt{-1}$). Boundary conditions (including considerations due to change in the effective mass across a boundary) relate $\phi_{j+1}^{\pm}$ for adjacent wells by 2×2 matrices $[\mathbf{S}]_j$ given by

$$\begin{pmatrix} \phi_j^+ \\ \phi_j^- \end{pmatrix} = [\mathbf{S}]_j \begin{pmatrix} \phi_{j+1}^+ \\ \phi_{j+1}^- \end{pmatrix} = \frac{k_j^* + k_{j+1}^*}{2k_j^*} \begin{pmatrix} \mathrm{e}^{-\mathrm{i}\delta_j} & \Gamma_j \mathrm{e}^{-\mathrm{i}\delta_j} \\ \Gamma_j \mathrm{e}^{\mathrm{i}\delta_j} & \mathrm{e}^{\mathrm{i}\delta_j} \end{pmatrix} \begin{pmatrix} \phi_{j+1}^+ \\ \phi_{j+1}^- \end{pmatrix} \tag{A2}$$

where

$$\delta_j = k_j d_j \qquad (\delta_1 = 0)$$
$$\Gamma_j = \frac{k_j^* - k_{j+1}^*}{k_j^* + k_{j+1}^*} \qquad \text{where } k_j^* = \frac{k_j}{m_j^*}.$$

From figure A1(a) we can identify ϕ_1^- as the amplitude reflection coefficient (r) and ϕ_N^+ as the amplitude transmission coeficient (t) and therefore, by multiplying $N - 1$ matrices, we get

$$\begin{pmatrix} 1 \\ r \end{pmatrix} = \prod_{j=1}^{N-1} [\mathbf{S}]_j \begin{pmatrix} t \\ 0 \end{pmatrix} = \begin{pmatrix} S_{11} & S_{12} \\ S_{21} & S_{22} \end{pmatrix} \begin{pmatrix} t \\ 0 \end{pmatrix}.$$

The particle's transmission coefficient, given by $T = |1/S_{11}|^2$, is evaluated as a function of the energy with which it is incident. In the limit of large barrier widths and a large number of approximating wells, the energies at which T peaks are the eigenstate energies in the well. The program written to do this calculation was tested with a finite parabolic potential

and, as shown in figure A1(b), the characteristic $(n+\frac{1}{2})\hbar\omega$ behaviour of the energy spectrum for the low-lying levels is quite clearly evident.

References

[1] Deppe D G and Holonyak N 1988 *J. Appl. Phys.* **64** R93
[2] Egger U, Schultz M, Werner P, Breitenstein O, Tan T Y, Gosele U, Franzheld R, Uematsu M and Ito H 1997 *J. Appl. Phys.* **81** 6056
[3] Gillin W P, Sealy B J and Homewood K P 1991 *Opt. Quantum Electron.* **23** 975
[4] Camras M D, Holonyak N Jr, Burnham R D, Streifer W, Scifres D R, Paoli T L and Lindstrom C 1983 *J. Appl. Phys.* **54** 5637
[5] Pollak F H and Shen H 1993 *Mater. Sci. Eng.* R **10** 275
[6] Yin X and Pollak F H 1991 *Appl. Phys. Lett.* **59** 2305
[7] Ghosh S and Arora B M 1996 *Proc. Int. Conf. on Instrumentation* ed B S Ramprasad, S Asokan, K Rajanna and N C Shivaprakash (Bangalore: New Age)
[8] Casey H C Jr and Panish M B 1978 *Heterostructure Lasers* Part B (New York: Academic)
[9] Pollak F H 1990 *Semiconductors and Semimetals* vol 32, ed T P Pearsall (New York: Academic)
[10] Madelung O, von der Osten W and Rossler U (ed) 1987 *Landolt–Börnstein New series* Group III, vol 22a (Berlin: Springer)
[11] Prins A D, Dunstan D J, Lambkin J D, O'Reilly E O, Adams A R, Pritchard R, Truscott W S and Singer K E 1993 *Phys. Rev.* B **47** 2191
[12] Lankes S, Hahn B, Meier C, Hierl F, Kastner M, Rosenauer A and Gebhardt W 1995 *Phys. Status Solidi* a **152** 123
[13] Khreis O M, Gillin W P, Homewood K P and Singer K E 1998 *J. Appl. Phys.* **84** 4017
[14] Gillin W P, Rao S S, Bradley I V and Homewood K P 1993 *Appl. Phys. Lett.* **63** 797
[15] Palfrey H D, Brown M and Willoughby A F W 1983 *J. Electron. Mater.* **12** 864
[16] Tsang J S, Lee C P, Lee S H, Tsai K L, Tsai C M and Fan J C 1996 *J. Appl. Phys.* **79** 664
[17] Rao S S, Gillin W P and Homewood K P 1994 *Phys. Rev.* B **50** 8071
[18] Ghatak A K, Thyagarajan K and Shenoy M R 1988 *IEEE J. Quantum Electron.* **24** 1524